Continuous isolated noise sources induce repeating waves in the coda of ambient noise correlations

S. Schippkus * [1], **M. Safarkhani** [1], **C. Hadziioannou** [1]

[1]Institute of Geophysics, Centre for Earth System Research and Sustainability (CEN), Universität Hamburg, Hamburg, Germany

Author contributions: *Conceptualization*: SS, MS, CH. *Methodology*: SS. *Software*: SS. *Data curation*: MS. *Formal Analysis*: SS. *Investigation*: SS, MS. *Resources*: SS, CH. *Writing - original draft*: SS. *Writing - Review & Editing*: SS. *Visualization*: SS. *Supervision*: CH. *Funding acquisition*: SS,CH.

Abstract Continuous excitation of isolated noise sources leads to repeating wave arrivals in cross correlations of ambient seismic noise, including throughout their coda. These waves propagate from the isolated sources. We observe this effect on correlation wavefields computed from two years of field data recorded at the Gräfenberg array in Germany and two master stations in Europe. Beamforming the correlation functions in the secondary microseism frequency band reveals repeating waves incoming from distinct directions to the West, which correspond to well-known dominant microseism source locations in the Northeastern Atlantic Ocean. These emerge in addition to the expected acausal and causal correlation wavefield contributions by boundary sources, which are converging onto and diverging from the master station, respectively. Numerical simulations reproduce this observation. We first model a source repeatedly exciting a wavelet, which helps illustrate the fundamental mechanism behind repeated wave generation. Second, we model continuously acting secondary microseism sources and find good agreement with our observations. Our observations and modelling have potentially significant implications for the understanding of correlation wavefields and monitoring of relative velocity changes in particular. Velocity monitoring commonly assumes that only multiply scattered waves, originating from the master station, are present in the coda of the correlation wavefield. We show that repeating waves propagating from isolated noise sources may dominate instead, including the very late coda. Our results imply that in the presence of continuously acting noise sources, which we show is the case for ordinary recordings of ocean microseisms, velocity monitoring assuming scattered waves may be adversely affected with regard to measurement technique, spatial resolution, as well as temporal resolution. We further demonstrate that the very late coda of correlation functions contains useful signal, contrary to the common sentiment that it is dominated by instrument noise.

Non-technical summary Seismic waves are generated by all kinds of sources, including earthquakes, ocean waves, and machinery. Some sources produce a consistently present background level of seismic energy, so-called ambient seismic noise. It is well-established that, under

*Corresponding author: sven.schippkus@uni-hamburg.de

the condition of evenly distributed noise sources, cross-correlation of ambient seismic noise, which was recorded on two separate seismic stations, yields a new wavefield that propagates directly from one station to the other. We call this new wavefield the correlation wavefield. Here, we show that in the presence of an additional isolated noise source that excites seismic waves continuously, for example ocean waves induced by storm systems over the Northeastern Atlantic, a new contribution to the correlation wavefield emerges: repeating waves propagating from the isolated noise source. These repeating waves can be more coherent across several stations than the expected correlation wavefield contribution, which propagates from one station to the other. We observe such repeating waves propagating from isolated noise sources on correlation wavefields computed from two years of seismic recordings of the Gräfenberg seismic array in Germany and two master stations in Europe. We reproduce our observations with numerical simulations of the sources and resulting correlation wavefields. Our findings have potentially significant implications for seismic monitoring based on relative velocity changes, which is used to monitor geological faults, volcanoes, groundwater, and other processes in the Earth. Velocity monitoring commonly relies on the assumption that the correlation wavefield contains only the contribution that propagates from one station to the other, which we show is not necessarily correct. This can lead to misinterpretation of measured velocity variations.

1 Introduction

Seismic interferometry of the ambient seismic field gives rise to new correlation wavefields that relate to the Green's function under the condition of uniformly distributed noise sources (Wapenaar et al., 2005; Gouédard et al., 2008). These correlation wavefields are now routinely used for imaging (e.g., Schippkus et al., 2018; Lu et al., 2018) and monitoring (e.g., Wegler and Sens-Schönfelder, 2007; Hadziioannou et al., 2009; Sheng et al., 2023) of Earth's structure. In the presence of an isolated noise source, a second contribution to this wavefield is introduced, sometimes referred to as spurious arrival (Snieder et al., 2006; Zeng and Ni, 2010; Retailleau et al., 2017; Schippkus et al., 2022). This correlation wavefield contribution can lead to biased measurements of seismic wave speed due to interference of direct waves from the master station and the isolated noise source (Schippkus et al., 2022).

Monitoring applications, on the other hand, rely on estimating relative velocity changes by repeatedly computing correlation wavefields throughout time and measuring changes in the arrival time of their coda (Wegler and Sens-Schönfelder, 2007; Sens-Schönfelder and Larose, 2010). Current strategies often rely on the assumption that the coda of a given correlation wavefield is comprised of multiply scattered waves, originating from the master station, which also dictates its spatial sensitivity (Planès et al., 2014; Margerin et al., 2016; van Dinther et al., 2021). If the spatial sensitivity of the coda is known, seismic velocity changes can be located (Obermann et al., 2014; Mao et al., 2022). Some progress has been made in accounting for the impact of changes in sources on the correlation wavefield, particularly in the context of monitoring at frequencies above 1 Hz, e.g., by carefully selecting time windows in which the same sources are active and produce similar correlation wavefields (Yates et al., 2022; Sheng et al., 2023).

In this study we demonstrate that isolated noise sources may impact correlation wavefields to a degree previously not considered. Continuously acting isolated noise sources, such as ocean microseisms, produce repeating waves throughout the entire correlation function that propagate from the isolated source location. These waves coincide with and are more coherent than multiply scattered waves originating from the master station. This may have significant impact on the understanding of measured velocity changes. In the following, we show observations of these repeating waves on field data correlation functions in the ocean microseism frequency band using stations throughout Europe, illustrate the mechanism behind repeated direct-wave generation in correlation functions, and finally reproduce our field data observations by modelling continuously acting isolated noise sources, i.e., secondary ocean microseisms.

2 Beamforming the correlation wavefield

We compute correlation wavefields from two years of continuous vertical component seismograms, recorded in 2019 and 2020 at the Gräfenberg array in Germany and two master stations, IV.BRMO in Italy (Fig. 1a) and PL.OJC in Poland (Fig. 2a). IV.BRMO was chosen randomly and PL.OJC was chosen to showcase a different backazimuth and slightly larger distance to the Gräfenberg array. We apply a standard processing workflow: remove instrument response, cut two years of data into two-hour long segments overlapping by 50%, apply spectral whitening (Bensen et al., 2007), cross-correlate each segment, and stack all segments linearly. No further processing, e.g., earthquake removal or other segment selection, has been applied, because whitening in each segment already normalises the energy potentially introduced by earthquakes and we find no evidence for earthquakes-related bias in the resulting correlation wavefields.

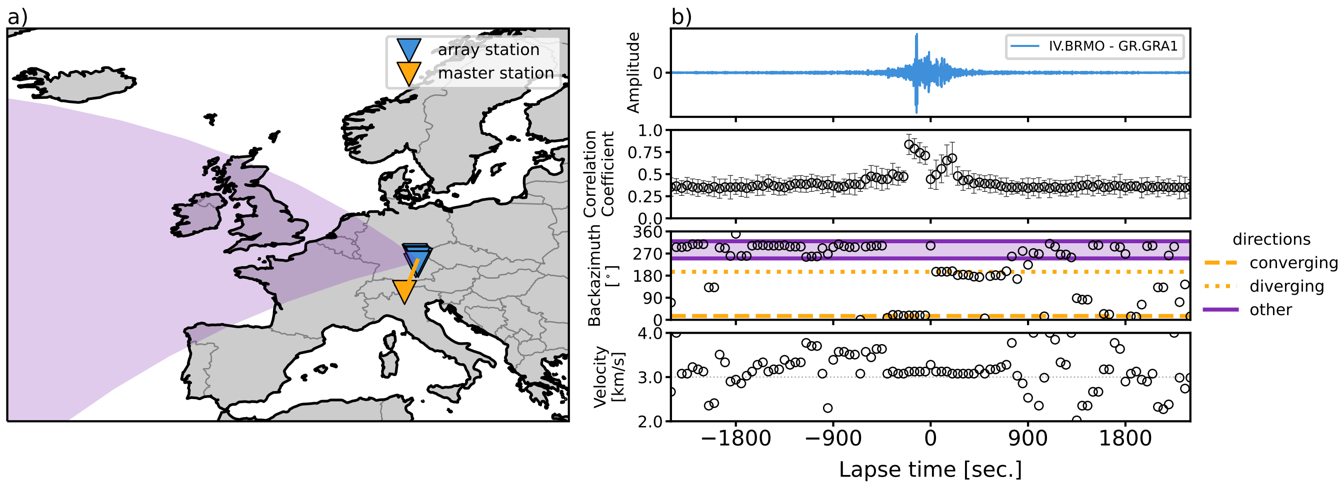

Figure 1 Beamforming the correlation wavefield between the Gräfenberg array in Germany (blue triangle) and master station IV.BRMO, Italy (yellow triangle), in the secondary microseism frequency band (0.1 to 0.3 Hz). a) Overview map with master station and array stations. The orange line and purple area correspond to the dominant directions detected by beamforming. b) Beamforming results: sample cross-correlation between the master station and one array station (top), mean Pearson correlation-coefficient of correlation functions with best-fitting beams in each window (second panel), detected direction of arrival (third panel), and estimated phase velocity (bottom). Detected directions correspond to the correlation wavefield converging onto and diverging from the master station (orange lines), and a range of directions pointing towards the Atlantic Ocean (purple area).

To estimate from which directions the correlation wavefield arrives at the Gräfenberg array, we beamform the correlation functions (Fig. 1). We beamform in 200 sec. windows, overlapping by 75%, in the secondary micro-

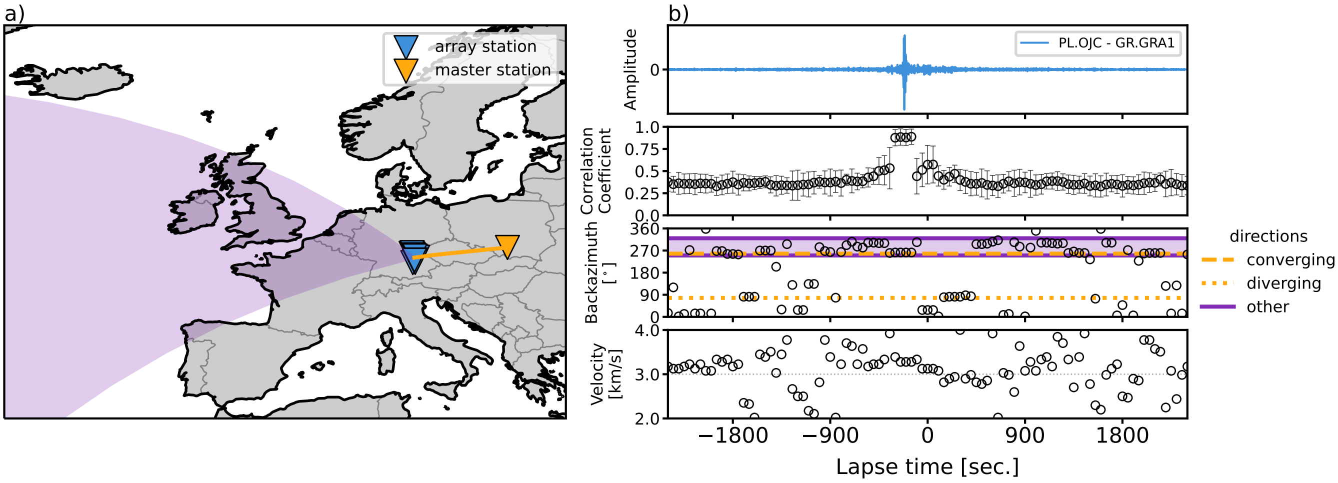

Figure 2 Same as Figure 1, but for master station PL.OJC, Poland. The directions detected by beamforming corresponding to the diverging and converging part of the correlation wavefield change with master station as expected (orange lines), whereas the range of directions towards the Northern Atlantic remains constant (purple area). Note that the converging part of the correlation wavefield points towards West, similar to one of the dominant directions detected pointing towards the Atlantic Ocean for master station IV.BRMO (Fig. 1).

seism frequency band (0.1 to 0.3 Hz), and assuming plane-wave propagation (Rost and Thomas, 2002). We present a sample correlation function to give orientation in lapse time (Fig. 1b, top panel), and compute Pearson correlation coefficients of all correlation functions with the best-fitting beam for each window to estimate how well the beam explains the data within a window (Fig. 1b, second panel). Similarity is highest for the expected acausal arrival, which also emerges more clearly in the correlation function than the causal arrival, due to the commonly observed strong noise sources in the Northeastern Atlantic (e.g., Friedrich et al., 1998; Chevrot et al., 2007; Juretzek and Hadziioannou, 2016). Throughout the coda, similarity remains nearly constant with a correlation coefficient ~ 0.4. We detect several dominant directions of arrival (Fig. 1b, third panel). First, the acausal arrival of the correlation wavefield converging onto the master station at negative lapse time (dashed orange line) and the causal arrival diverging from the master station at positive lapse time (dotted orange line), i.e., the correlation wavefield contribution that usually arises in seismic interferometry (Wapenaar et al., 2005). Second, distinct directions throughout the correlation functions pointing towards West (Fig. 1b, third panel), which we project onto the map view (Fig. 1a).

A second master station in Poland (PL.OJC) illustrates how the converging (acausal) and diverging (causal) parts of the correlation wavefield depend on the geometry of array stations to master station and point roughly towards the great-circle between the two (Soergel et al., 2022), whereas the dominant directions towards West appear to be independent of the master station (Fig. 2). A North-Northeast direction, however, still emerges in the beamforming results as most coherent, which coincides approximately with the great circle direction for the converging part of the correlation wavefield for master station IV.BRMO (Fig. 1). Similarly, the converging direction for master station PL.OJC coincides with the dominant directions towards West (Fig. 2). This hints at the impact the geometry of master station and array stations has on the detection and identification potential of these other directions. We propose the dominant directions detected by beamforming and pointing towards West represent repeating direct waves emerging at isolated noise source locations in the Northeastern Atlantic Ocean. The North-Northeasterly direction observed in the coda in both examples similarly represents waves arriving from isolated source locations off the coast of Norway, which were previously observed as dominant on continuous seismograms (e.g., Juretzek and Hadziioannou, 2016).

We call these direct waves, because they propagate directly from the isolated source to the seismic stations. These are not to be confused with the direct waves propagating between the stations, i.e., the expected acausal and causal arrivals.

3 A repeating impulsive isolated noise source

To substantiate our hypothesis and explain the observations above, we start from the concept of an isolated noise source (Schippkus et al., 2022). Consider a wavefield that is excited by sources on a boundary S and an isolated noise source at $\mathbf{r}_N$, recorded on a station at location $\mathbf{r}$

$$u(\mathbf{r}) = \oint_S N_B(\mathbf{r}')G(\mathbf{r}, \mathbf{r}')d\mathbf{r}' + N_I G(\mathbf{r}, \mathbf{r}_N) \ , \tag{1}$$

with G the Green's function and N_B and N_I the source spectra of boundary sources and the isolated source, respectively. This section is formulated in the frequency domain. The cross-correlation of this wavefield at location $\mathbf{r}$ with the wavefield recorded on a master station at $\mathbf{r}_M$ is given by (eq. 6 of Schippkus et al., 2022)

$$\langle u(\mathbf{r})u^*(\mathbf{r}_M)\rangle = \frac{\rho c|N_B|^2}{2} \left(G(\mathbf{r}, \mathbf{r}_M) + G^*(\mathbf{r}, \mathbf{r}_M)\right) + |N_I|^2 G(\mathbf{r}, \mathbf{r}_N)G^*(\mathbf{r}_M, \mathbf{r}_N) \ , \tag{2}$$

with ρ the mass density of the medium and c the propagation velocity. The first term describes the contribution of uncorrelated sources on the boundary S surrounding the stations, which usually arises in seismic interferometry (as in Wapenaar et al., 2005), and the second term describes the contribution of the isolated noise source. The relation of these terms has been investigated by Schippkus et al. (2022), who demonstrate how the direct arrivals of these two wavefield contributions interfere for certain station geometries, leading to biased surface wave dispersion measurements. In their modelling, the authors assumed the source term of the isolated source N_I to be a wavelet, excited once.

Here, we expand upon this idea by considering the isolated noise source to be excited multiple times in a correlated manner. For illustration purposes, we express its source term as $N_I = W_I E_I$, with a wavelet W_I and excitation pattern E_I. The contribution of the isolated noise source to the correlation wavefield is hence

$$|W_I|^2|E_I|^2 G(\mathbf{r}, \mathbf{r}_N)G^*(\mathbf{r}_M, \mathbf{r}_N) \ . \tag{3}$$

A simple example of an isolated noise source exciting a Ricker wavelet, repeating 5 times with a 20 sec. interval, illustrates how such a source manifests in correlation functions (Fig. 3). For such a source, the excitation pattern is a time series with 1 at every interval of 20 sec. (5 times), and 0 elsewhere. The auto-correlation of the wavelet $|W_I|^2$ (Fig. 3a), auto-correlation of the excitation pattern $|E_I|^2$ (Fig. 3b), and cross-correlation of the Green's functions $G(\mathbf{r}, \mathbf{r}_N)G^*(\mathbf{r}_M, \mathbf{r}_N)$ for surface waves in a homogeneous, isotropic, acoustic medium and an arbitrary geometry (Fig. 3c) are convolved to result in a repeating wavelet with the same 20 sec. interval, present in the correlation wavefield (Fig. 3d). These repeating wavelets represent direct waves emitted from the isolated source location.

A sketch of the correlation wavefield in the presence of a repeating impulsive isolated noise source helps illustrate

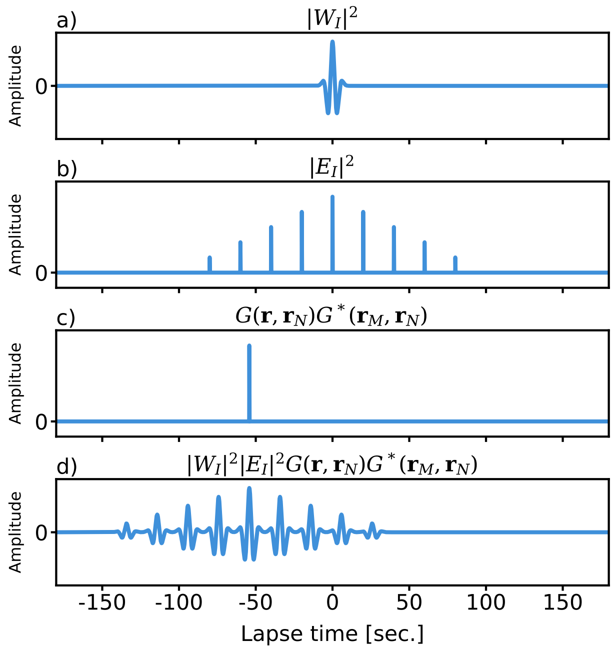

Figure 3 A repeating isolated noise source produces repeating direct waves in correlation functions, depicted in time domain. a) Auto-correlation of the wavelet $|W_I|^2$. b) Auto-correlation of the excitation pattern $|E_I|^2$ with a regular 20 sec. interval, excited 5 times. Note that amplitudes decay by $1/5$ every interval away from 0 sec. lapse time. c) Cross-correlation of the Green's functions between the isolated noise source and both station locations for an arbitrary geometry. d) Second term of the correlation wavefield (eq. 3, the convolution of a-c), where each arriving wavelet represents a direct wave emitted from the isolated noise source at $\mathbf{r}_N$.

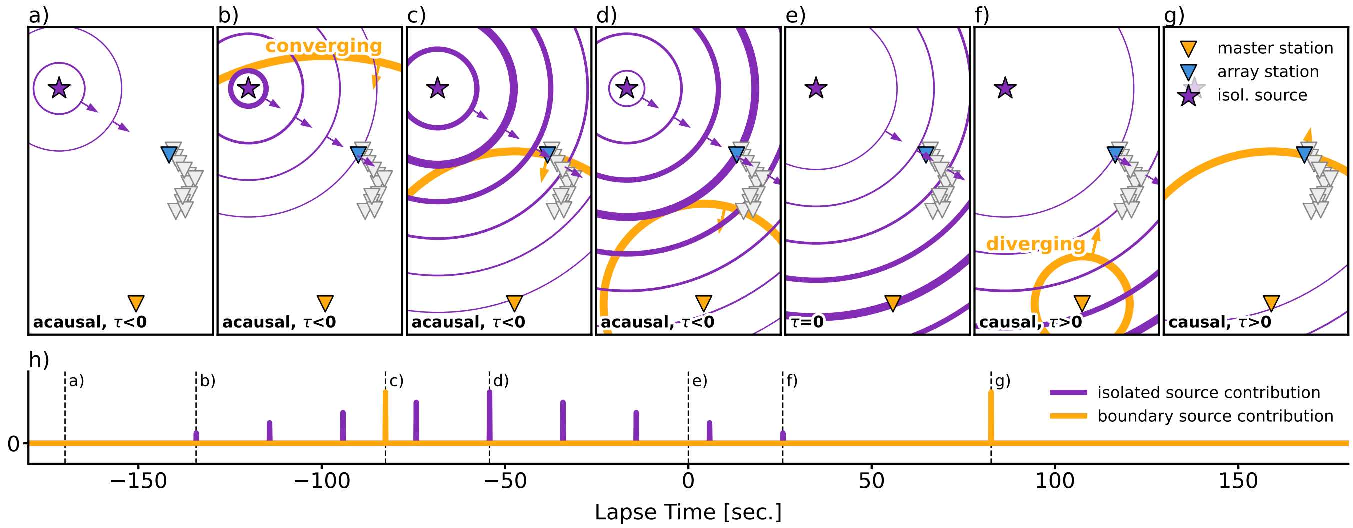

Figure 4 Schematic illustration of the correlation wavefield in the presence of a repeating impulsive source (5 excitations, 20 sec. interval, same as in Figure 3). We remove the wavelet for improved clarity. a-g) Snapshots of the correlation wavefield at different lapse times, indicated by dashed lines in h). The contributions of the isolated source (purple lines) and boundary sources surrounding the master and array stations (yellow line) propagate through the medium. Line thickness indicates amplitude. h) Correlation function between the array station and the master station, color-coded by isolated source and boundary source contribution (purple and yellow, respectively). Dashed vertical lines mark the lapse time snapshots displayed in a-g. The acausal part of the correlation function contains repeating waves propagating from the isolated source and the boundary source contribution converging onto the master station (a-d). At lapse time $\tau = 0$, both the main arrival of the isolated source contribution and the boundary source contribution reach the master station (e). At causal lapse time, the last arrivals of the isolated source reach the array station (f) and finally the diverging contribution of the boundary sources (g).

its evolution with lapse time (Fig. 4). The wavefield is comprised of the two contributions by boundary sources (first term of eq. 2, yellow in Fig. 4) and the isolated noise source (eq. 3, purple in Fig. 4). The boundary source contribution converges onto the master station at negative lapse times (the acausal part), and diverges from the station at positive lapse times (the causal part, Fig. 4a-g). This is the expected contribution that usually arises in seismic interferometry. The repeating isolated noise source induces waves that emerge earlier and with lower amplitude than the main arrival (Fig. 4a) and eventually reach the array station (4b). The main arrival (highest amplitude, indicated by line thickness) of the isolated noise source emerges at $\tau = -|\mathbf{r}_M - \mathbf{r}_N|/c$ and touches the boundary source contribution along the line connecting the isolated source and master station (c-f, as in Schippkus et al., 2022). At lapse time $\tau = 0$, both the wavefield contribution by boundary sources and the main arrival of the isolated noise source reach the master station (Fig. 4e). At causal lapse times, the last repeating waves from the isolated noise source reach the array station (Fig. 4f) before the boundary source contribution diverging from the master station arrives at the at array station (Fig. 4g). The exact timing of each arrival depends on the geometry of isolated source, master station, and array stations, as well as the excitation pattern.

Note that the repeating direct waves from the isolated noise source are asymmetrical in lapse time (Figs. 3, 4), because there is no part of the correlation wavefield converging onto the isolated noise source (Schippkus et al., 2022). How strongly these repeating direct waves manifest depends on how highly correlated the isolated source is with itself throughout time. The example presented here constitutes the most extreme case, i.e., identical wavelet and exactly regular excitation pattern. Even under these conditions, amplitudes decay linearly with time due to the finite length of the excitation pattern (Fig. 3b). In this example, the amplitude of the excitation pattern auto-correlation decreases by $1/5$ of the maximum amplitude with each interval away from 0 sec., because the source is excited 5 times. Slight variations in amplitude, shape of the wavelet, or excitation timing lead to reduced correlation, and thus repeating direct waves with reduced amplitude or different shape. If there was no correlation, the repeating waves would disappear. The main arrival would remain.

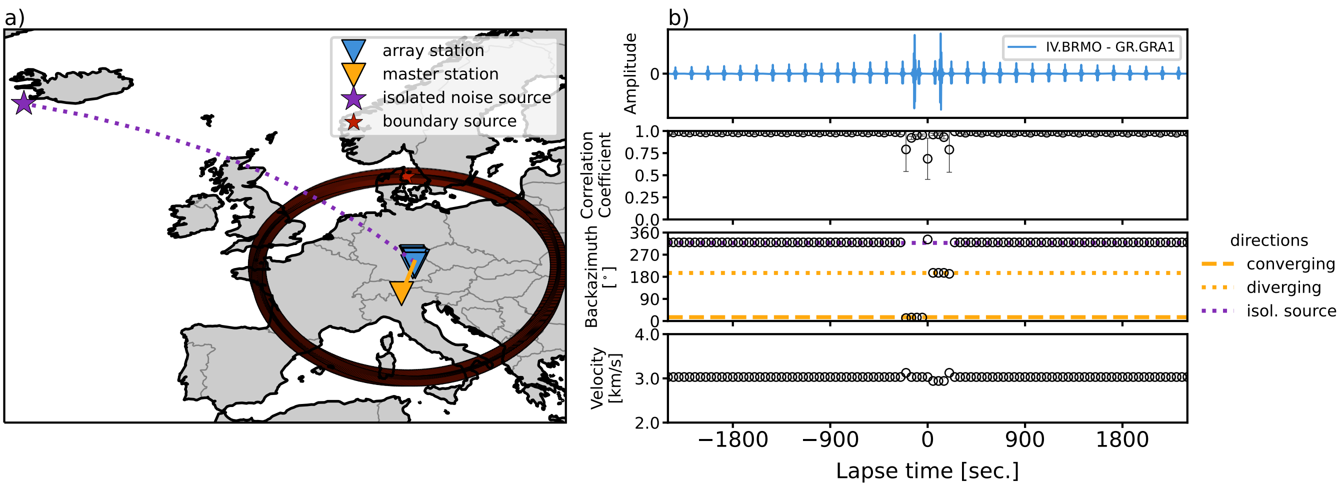

Figure 5 Beamforming synthetic cross-correlation functions detects repeating direct waves from the regularly repeating isolated noise source. a) Overview map: master station (orange triangle), array stations (blue triangle), boundary sources in a small circle surronding the stations (red stars) and the isolated noise source Southwest of Iceland (purple star). b) Beamforming results: sample cross-correlation between master station and one array station, mean correlation-coefficients between windowed correlation functions and beams, detected direction of arrival, and estimated phase velocity. The boundary source contribution to the correlation wavefield converging onto and diverging from the master station (orange lines, first term in eq. 2) is detected as well as repeating direct waves from the isolated noise source (purple line, second term in eq. 2).

To confirm the repeating wavelets in the correlation functions indeed represent repeating direct waves emitted from the isolated noise source, we model a master station in Italy (same location as IV.BRMO), array stations in Southern Germany (same locations as the Gräfenberg array), 1000 boundary sources surrounding the stations in a small-circle with 1000 km distance to them, as well as a repeating isolated noise source Southwest of Iceland (Fig. 5a). All sources excite Ricker wavelets, and only the isolated noise source repeats it 50 times with a 150 sec. interval (similar to Figs. 3, 4). We compute synthetic surface wave seismograms by assuming a homogeneous, isotropic, acoustic half-space with a medium velocity $v = 3$ km/s for simplicity (i.e., Green's functions are of the form $e^{-i\omega x/v}$), and compute cross correlations of those waveforms. During the calculations, we treat boundary sources and the isolated noise source separately in accordance with equation (2). The maximum amplitude of the isolated noise source contribution is scaled to $1/4$ of the boundary source contribution to distinguish them easily (Fig. 5b, top panel). The correlation wavefield contains both wavefield contributions. Beamforming the cross-correlation functions between the master station and all array stations detects three directions of arrival (Fig. 5b, third panel): the first term of the correlation wavefield converging onto the master station at negative lapse time (dashed orange line) and diverging from the master station at positive lapse time (dotted orange line), and repeating direct waves from the isolated source (purple dotted line) throughout the correlation function. The estimated phase velocity of $\sim$ 3 km/s is the medium velocity (Fig. 5b, bottom panel). Note that the correlation functions match exactly with the beam (correlation coefficent of 1) only for time windows that do not contain both contributions simultaneously (Fig. 5b, second panel).

This example illustrates the principle behind repeating direct waves emerging in correlation functions. However, we observed this effect on field data of secondary ocean microseisms (Figs. 1, 2), which are better described as continuously acting sources, which we introduce in the following.

4 Continuously acting isolated noise sources

To describe the suspected isolated noise source (Figs. 1, 2) as a continuously acting microseism source, we rely on the parametrization employed by Gualtieri et al. (2020) (eq. 3 therein). The surface pressure P at colatitude θ and longitude ϕ excited by the secondary microseism mechanism is described as a superposition of many harmonics

$$P(t, \theta, \phi) = \sum_{i=1}^{H} A(f_i, \theta, \phi) \cos(2\pi f_i t + \Phi_i), \tag{4}$$

with H the number of harmonics, A the amplitude of the harmonic frequency f_i, and $\Phi_i \in [0, 2\pi)$ its phase, sampled uniformly random. The amplitude A relates to the power spectral density of ocean gravity waves and incorporates local site effects, and is described in more detail by Gualtieri et al. (2020). For our considerations, we neglect the amplitude term ($A = 1$), because we investigate a fairly narrow frequency band and the exact amplitude of each harmonic is irrelevant for explaining the effect observed in this study. In the following, we use $P(\theta, \phi)$ (the spectrum of $P(t, \theta, \phi)$) with harmonics from 0.1 to 0.3 Hz directly as the source term N_I (Fig. 6a). Its auto-correlation (Fig. 6b), convolved with the same Green's function cross-correlation as above (Fig. 3c) contains one clear main arrival and weak, repeating direct waves (Fig. 6c). These repeating waves excited by a microseism source have much lower amplitude and inconsistent shape compared to a repeating impulsive isolated noise source (Fig. 3) due to decreased correlation of the source term with itself throughout time.

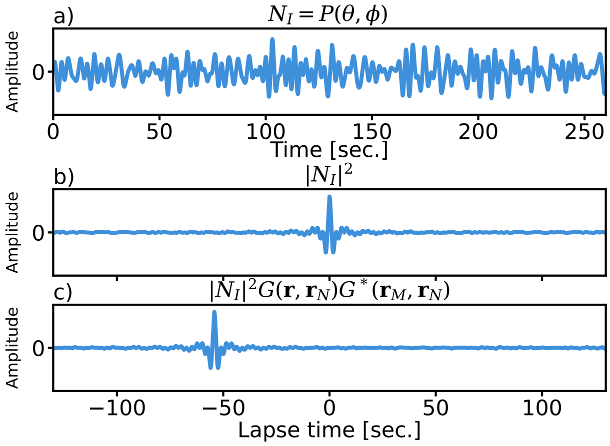

Figure 6 Contribution to the correlation wavefield by a continuously acting isolated noise source. a) Source term for a secondary microseism source, if all harmonics between 0.1 and 0.3 Hz are excited with a uniformly random phase $\Phi_i \in [0, 2\pi)$ and equal amplitude $A = 1$ (eq. 4). b) Auto-correlation of the source term $|N_I|^2$. c) Convolution of $|N_I|^2$ with the same Green's function cross-correlation as in Figure 3c, i.e., the second term of the correlation wavefield (eq. 2), with a main arrival and low-amplitude, repeating direct waves throughout the coda.

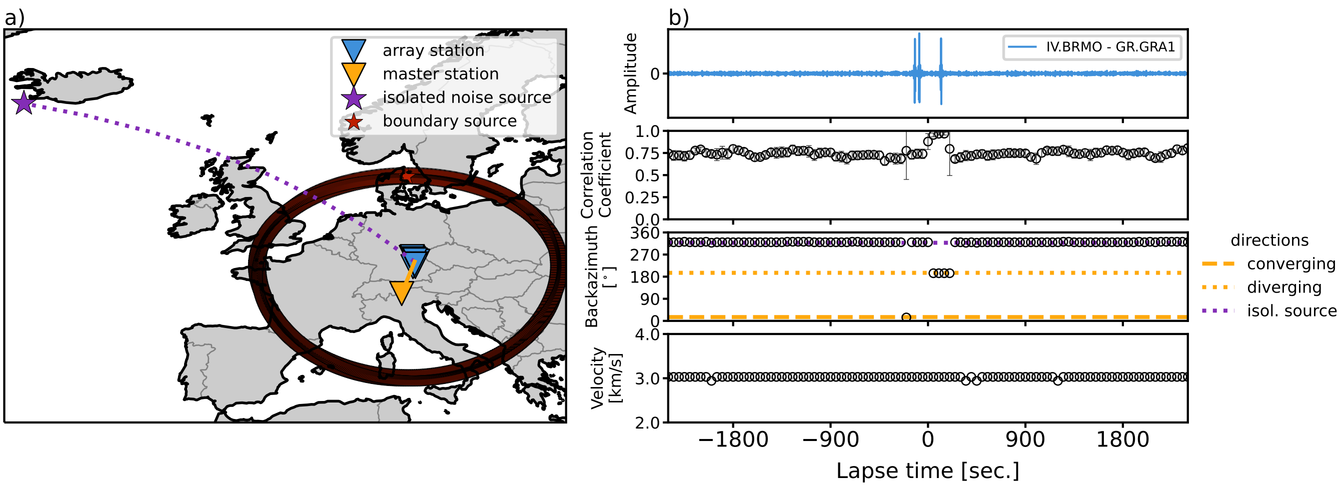

Figure 7 Same as Figure 5 but for secondary microseism source terms for both boundary and isolated sources. Both contributions to the correlation wavefield are scaled to have similar amplitudes. Distinct main arrival (the "spurious" arrival) of the isolated noise source at ~ -100 sec. lapse time. For this arrival and throughout the coda, direct waves from the isolated source are detected as most coherent.

We repeat the numerical simulation above (Fig. 5) with $P(\theta, \phi)$ as the source term for both boundary and isolated noise sources (Fig. 7). Both contributions to the correlation wavefield are scaled to have similar amplitudes. A secondary microseism source produces repeating direct waves in correlation wavefields (Fig. 7b), similar to the regularly repeating source (Fig. 5). Near the main arrival of the isolated source (at ~ -100 sec., after the acausal arrival due to boundary sources) and throughout the coda, repeating direct waves from the isolated noise source location are detected as most coherent. Distinct main arrivals (the "spurious" arrival) have been observed for localised microseism sources before (Zeng and Ni, 2010; Retailleau et al., 2017). These main arrivals must arrive in-between the acausal and causal arrivals of the boundary source contribution (Schippkus et al., 2022). In this study, we do not observe a particularly clear main arrival on field data (Figs. 1, 2). Still, the coda of the field data correlation

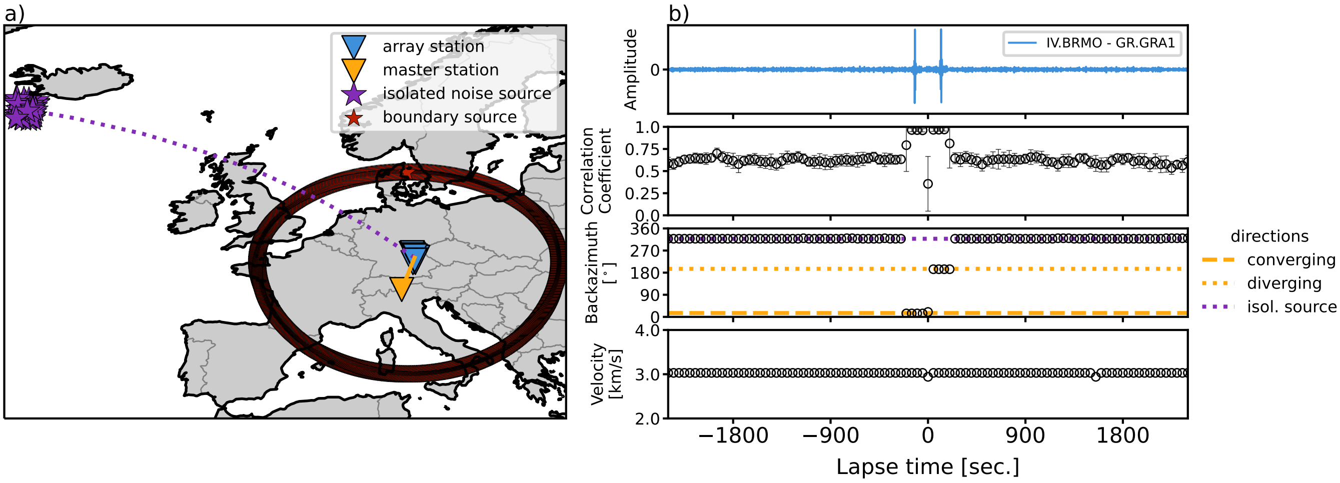

Figure 8 Same as Figure 7 but for a cluster of isolated sources. Amplitudes of the summed isolated noise source contribution is scaled to 1/10 of the boundary source contribution. No distinct spurious arrival but coda still dominated by repeating direct waves from the isolated noise source cluster.

wavefields appears to be dominated by repeating waves from isolated noise sources. Correlation coefficients of the synthetic correlation functions with the beams for each window reach ~ 1 for the main causal arrival, and ~ 0.75 for the acausal arrival due to interference with the isolated source arrival (Fig. 7b). Throughout the coda, correlation coefficients do not exceed 0.75 significantly, because continuously acting boundary sources also induce a repeating contribution in the correlation wavefield. In other words, the best beam does not represent the correlation functions entirely, even under the ideal conditions considered here, i.e., no heterogeneous structure, no dispersion, and no scattering.

To account for the fact we do not observe a distinct main arrival due to an isolated noise source in our field data correlations and to approximate a more realistic scenario by considering an extended source region, we place a cluster of 50 isolated noise sources Southwest of Iceland, each with a random realisation of the source term $P(\theta, \phi)$ and repeat the computations (Fig. 8). The wavefield contributions of those isolated noise sources, where each isolated source produces an additional term in equation (2), interfere to mask the main arrival (Fig. 8b). The amplitudes of the summed isolated noise source cluster contribution is scaled to $1/10$ of the boundary source contribution. Beamforming correlation functions again detects the converging and diverging part of the boundary source contribution, as well as the isolated noise source cluster as dominant throughout the coda (Fig. 8b). Correlation coefficients with the beams stabilise at ~ 0.65 in the coda, and are lower than for the case of a single source (Fig. 7b).

Finally, we place a second cluster of 50 isolated noise sources Northwest of the Iberian Peninsula (Fig. 9a) to account for the observation that within the range of directions toward the Northern Atlantic, two distinct directions appear to dominate (Figs. 1, 2). Both clusters of isolated noise sources are treated separately and their combined amplitudes are again scaled to $1/10$ of the boundary source contribution. Beamforming detects either one of the clusters as dominant, seemingly randomly throughout lapse time (Fig. 9b). Mean correlation coefficients with the beams are ~ 0.55 throughout the coda. This numerical simulation produces beamforming results closely resembling the measurements on field data correlation functions (Figs. 1, 2) and confirms that clusters of isolated noise sources produce repeating direct waves.

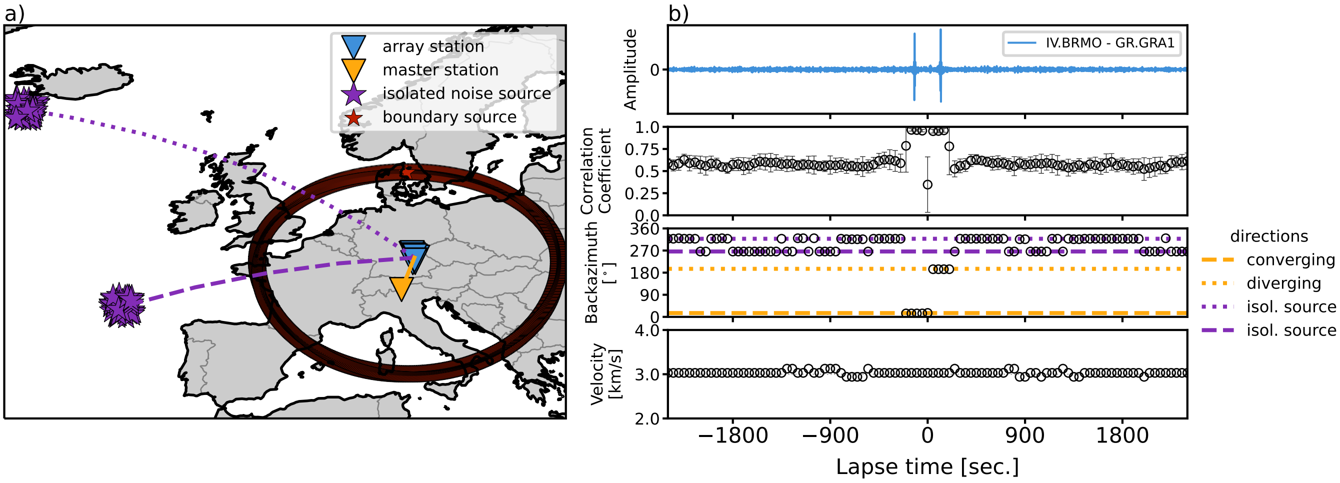

Figure 9 Same as Figure 8 but for two clusters of isolated noise sources. The additional cluster is placed Northwest of the Iberian Peninsula. The backazimuth to that cluster is indicated by a purple dashed line (a & b, third panel). Amplitudes of the isolated noise source contribution is scaled to $1/10$ of the boundary source contribution. No distinct spurious arrival. Beamforming detects either of the two clusters at a given lapse time in the coda as dominant.

5 Discussion

In this study, we observe repeating direct waves propagating from isolated noise sources in the coda of correlation functions. We reproduce the observations by numerical modelling of continuously acting isolated sources.

The most significant question our analysis raises is: are repeating direct waves from isolated noise sources more dominant than multiply scattered waves, originating from the master station, also for individual correlation functions? If they were, our observations would have far-reaching implications. Beamforming, however, only shows that the contribution by isolated noise sources is more coherent across an array of stations (Figs. 1, 2). It is not surprising that multiply scattered waves can be incoherent across an array. To address this aspect, we compute correlation coefficients of all correlation functions with the beam in each beamforming window. These reach 0.75 to 0.9 (never 1) for the expected stronger, coherent acausal arrival on field data correlations (Figs. 1, 2), which indicates that not all factors are accounted for during beamforming, namely heterogeneous structure, scattering, elastic wave propagation, and additional isolated sources. Still, these correlation coefficients provide a benchmark of what can be expected for the most coherent part of the correlation wavefield. In our numerical simulations, correlation coefficients are ~ 1 for the main arrivals without the interference of distinct spurious arrivals (Figs. 5, 7, 8, 9). Throughout the coda, we observe that correlation coefficients remain nearly constant for both the field data examples (~ 0.4, Figs. 1, 2) and the numerical simulations, decreasing with increasing complexity of the original wavefield from one isolated noise source (~ 0.75, Fig. 7), to a cluster of sources (~ 0.65, Fig. 8), to two clusters (~ 0.55, Fig. 9). Without taking into account the additional factors mentioned above (scattering, heterogeneous structure, or elastic waves), we reproduce a match between the modelled correlation functions and beams, comparable to the field data results. It is therefore reasonable to assume that the coda is not dominated by scattered waves, at least for absolute lapse times larger than a few hundred seconds.

At lapse times close to the direct arrivals from the master station (up to a few hundred seconds), correlation coefficients are higher than for the later coda and a transition to the stable regime observed in the later coda appears to manifest (Figs. 1, 2). In the early coda, scattered waves are likely dominant and thus also coherent in the correlation wavefield, although question arise about the degree of scattering. However, first tests on whether scattered waves are more coherent when the master station is much closer have shown no noticable difference in the beamforming results. The distinction between early coda and late coda arises, because amplitudes of the two correlation wavefield contributions decay for different reasons. Multiply scattered waves orginating from the master station decay due to attenuation during wave propagation, whereas repeating direct waves from isolated noise sources decay only due to correlation of the source term with itself through time (Figs. 3,6). As demonstrated above, even under ideal circumstances, amplitudes of repeating direct waves in correlation functions decay due to the finite length of the source and signal considered (Fig. 3).

In the later coda (absolute lapse times larger than a few hundred seconds), the commonly held assumption that the coda of a correlation wavefield is comprised dominantly, or even exclusively, of multiply scattered waves appears to be false. The beams pointing towards isolated noise sources represent a significant fraction of the correlation wavefield coda (Figs. 1, 2). Instead of spatially sampling the medium in a statistical manner (Margerin et al., 2016), the late coda, and thus measured velocity changes, may be dominantly sensitive to the path from the isolated noise source to the array station. Here, it is important to be clear about the nature of the coda and measurement principle. In the standard coda wave interferometry model, coda waves originate from the master station, are multiply scattered, and eventually reach the other receiver. A measured velocity change is then sensitive to this entire path. Because there is no clear way to know where exactly the wave has been and thus where the change has happened, recently developed coda wave sensitivity kernels are statistical descriptions of where the wave might have been, depending on the scattering properties of the medium (Margerin et al., 2016). However, if one would repeat the beamforming measurement described above, e.g., daily, to estimate the velocity of seismic waves in the coda, a potential velocity variation of those waves over time would have happened within the array, assuming constant sources. The standard coda wave interferometry measurement, in contrast, is performed on single correlation functions. If the measurement is performed in some part of the coda where repeating waves by isolated sources dominate, velocity variations may then be sensitive to the entire propagation path from isolated source to receiver, similar to the case where the coda is dominated by scattered waves and the sensitivity is along the path from master station to receiver. The difference here lies in the origin of the correlation wavefield contribution probed during the measurement and the ability to constrain the velocity change spatially. The main hypothesis in this paper is that the repeating waves we observe in beamforming originate from the isolated source, not the master station (Fig. 4).

A similar effect occurs in the presence of a strong nearby scatterer (van Dinther et al., 2021). As the multiply scattered part of the correlation wavefield reaches the strong scatterer, spatial sensitivity focuses along the path between stations and scatterer. In other words, the scatterer "emits" a direct wave, induced by the master station, that is recorded in the coda of the correlation function. This principle is similar to our considerations here, with the major difference that, in the modelling of van Dinther et al. (2021), the direct wave propagating from the scatterer originates from the master station. For isolated noise sources, direct waves originate from the source. The master station has no impact on the isolated source contribution to the correlation wavefield, as long as it coherently records the same isolated noise sources as the array stations, as the two field data examples suggest (Figs. 1, 2). We have no reason to suspect a strong scatterer to the West of the Gräfenberg array that could explain our measurements. Instead, our measurements are consistent with repeating direct waves from isolated noise sources, and reproduced by modelling without considering any scatterers. This means that different station pairs do not lead to different spatial sensitivity when recording such repeating direct waves. In some contexts, this may be advantageous by allowing repeated measurement of a repeating or continuous isolated source by considering multiple master stations. In the context of seismic monitoring of relative velocity variations, the impact of such sources has to be carefully considered.

The presence of repeating direct waves in the very late coda (30 minutes and more) furthermore challenges the common assumption that the very late coda of correlation wavefields is dominated by instrument noise and contains no useful signal. The very late coda is commonly used as a noise window for the estimation of signal-to-noise ratios of correlation functions, also for coda windows. We show that the very late coda does instead contain useful information, because repeating direct waves from isolated noise sources are still detected by beamforming (Figs. 1, 2). This also suggests amplitudes decay only slowly due to low correlation of the isolated source with itself over time (compared to Fig. 3), at least for the correlation wavefields investigated here, which were stacked over two years.

The early coda of correlation wavefields likely contains a significant contribution of scattered waves, as well as direct repeating waves from isolated noise sources. This suggests great care should be taken in measuring velocity variations and attributing them spatially also for the early coda. Common strategies to measure velocity variations, e.g., the stretching method (Lobkis and Weaver, 2003), assume that absolute timing delays increase with lapse time, because the seismic waves spent more time in the changed medium. For the contribution by repeating direct waves, stretching should not occur since absolute time delays are likely constant throughout the coda, as long as the isolated source does not change. A strategy that involves estimating the degree of stretching throughout the coda may give insight into the dominant regime (scattered waves vs. repeating waves) and whether the measurement approach is applicable. A different strategy to discriminate the correlation wavefield contributions may be to include measurements of wavefield gradients, which allow to separate the seismic wavefield using only single stations Sollberger et al. (2023).

Further questions arise about the temporal sensitivity of measured velocity variations. When considering scattered waves in the coda, velocity variation measurements are usually attributed to the entire time window used for correlation, e.g, a single measurement that represents an entire day. Repeating direct waves from isolated noise sources should in principle allow to improve temporal resolution, because arrivals at different lapse times likely have different temporal sensitivity in raw signal time domain, i.e., at what points in time the raw signal was recorded. However, it is not immediately obvious what time exactly a specific repeated arrival is sensitive to. This is a target for future studies.

Pre-processing of seismic records before cross-correlation plays an important role when investigating cross correlations of ambient seismic noise. We apply spectral whitening, a commonly adopted pre-processing strategy (Bensen et al., 2007). Spectral whitening is the normalisation of the amplitude spectrum before cross-correlation, often with a water level or smoothed spectrum to avoid introducing artefacts. Whitening is often successful in suppressing the impact of near-monochromatic signals, e.g., in the context of the 26 sec. microseism in the Gulf of Guinea (Bensen et al., 2007; Bruland and Hadziioannou, 2023) or wind turbine noise (Schippkus et al., 2022). On the other hand, whitening will also emphasise signals with relatively low amplitude in the original data. To confirm that our inter-

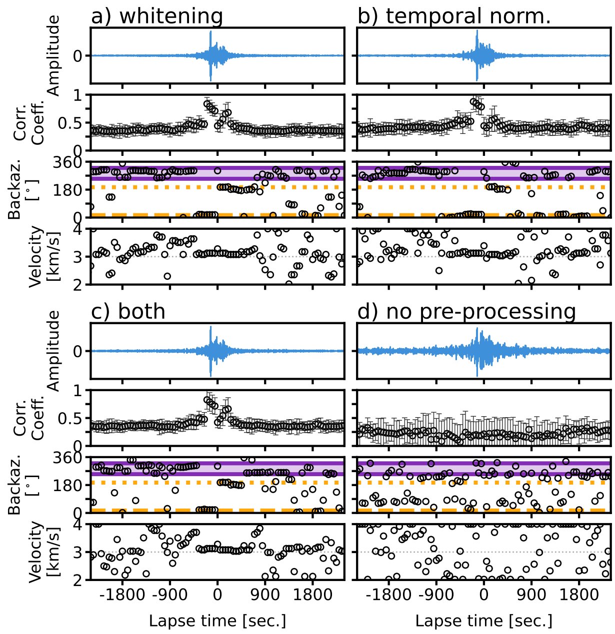

Figure 10 Impact of pre-processing scheme on the detection of repeating direct waves for master station IV.BRMO. a) Same as Figure 1b. b) Sample correlation function and beamforming result, if only temporal normalisation is applied. c) Results when both whitening and temporal normalisation are applied. d) Results when neither pre-processing is applied.

pretation of the results above is not significantly biased by the processing strategy, we repeat the measurements for master station IV.BRMO (Fig. 1) with temporal normalisation, both whitening and temporal normalisation, and neither pre-processing (Fig. 10). Temporal normalisation (running window average) is performed in a 5 sec. moving window. As long as any processing to stabilise the correlation functions is applied (Fig. 10a-c), the fundamental observation of repeating direct waves remains. Slight differences emerge in the correlation functions themselves, and also which direction and velocity are detected at a given lapse time. Temporal normalisation is commonly applied in studies that measure relative velocity variations, often in its most extreme version one-bit normalisation. Here we demonstrate that common pre-processing schemes produce correlation functions with repeating direct waves. Without any processing, however, results become unstable and beamforming neither detects stable directions of arrival nor gives consistent phase velocity estimates (Fig. 10d). Correlation functions are more stable after such pre-processing, as is commonly observed, because these approaches (in addition to addressing some data glitches) reduce the impact of certain isolated noise sources on the recorded wavefield, in particular from transient high-amplitude sources (e.g., earthquakes) and continuous near-monochromatic sources (e.g., machinery). The sources that remain as dominant, after this pre-processing is applied, are continuously acting broadband sources (e.g., ocean microseisms) as is confirmed by beamforming (Figs. 1 & 2).

The temporal stability of ocean microseism sources that we impose in our modelling has been observed on field data correlations before. Zeng and Ni (2010) computed and stacked correlations over one year that show clear spurious energy due to a localized microseism source in Japan. Similarly, Retailleau et al. (2017) found localized microseism sources off the coasts of Iceland and Ireland, also in correlations stacked over one year. It may be unintuitive that ocean microseisms, often assumed to be a largely random process, would show any coherence at all. These previous and our results are clear indications that indeed the secondary microseism mechanism generates coherent sources that are somewhat stable over time. We are, however, not aware of a microseism source model that incorporates all these factors satisfactorily. Instead, we follow the current standard formulation, i.e., each frequency is excited with random but constant phase (Gualtieri et al., 2020). Investigations on how varying temporal source stability and stacking influence the beamforming detections or measured velocity changes will likely be part of future work.

It may also be surprising that the highly idealised Earth model employed in our simulations, i.e., Green's functions in an acoustic homogeneous half-space, is sufficient to reproduce our observations on field data to first order. We do not take any elastic wave propagation effects such as scattering into account. This suggests that these effects certainly present in real Earth structure and thus field data may play a less important role than often thought, at least for the specific case investigated here: the nature of the coda of ambient noise correlations.

Machinery- or traffic-based monitoring of velocity variations is likely similarly affected by the findings in this study. Rotating machinery, such as generators in wind turbines (Friedrich et al., 2018; Schippkus et al., 2020; Nagel et al., 2021), likely have source terms that are significantly correlated throughout time due to their mechanism, with higher correlation than ocean microseisms. These sources could produce repeating direct waves with high amplitude. Traffic, e.g., trains repeatedly passing the same spot, resembles repeatedly acting noise sources (as in Fig. 3), although with more complex wavelets and longer intervals. In case of traffic at a regular interval, e.g., trains on a schedule, the late coda of the correlation wavefield could allow to extract their signature reliably. Recently, approaches that identify and select appropriate time windows to use for cross-correlation and subsequent velocity monitoring have emerged (e.g., Yates et al., 2022; Sheng et al., 2023). These approaches are motivated by the realisation that correlation wavefields can be highly complex and depend significantly on the presence of isolated noise sources, similar to this study. Still, our findings also have impact on these strategies. In time windows where an isolated noise source is known to be particularly active, repeating direct waves may still emerge and coincide with the coda of that source, depending on the source signature and length of time window considered for cross-correlation. Further investigations on this aspect may help improve the accuracy of detected velocity changes in time and space.

6 Conclusion

Continuously acting isolated noise sources generate repeating direct waves that may dominate the coda of correlation wavefields, as observed on field data correlations (Figs. 1, 2) and reproduced by numerical simulations (Figs. 3-9). In the simulations, we start from the established concept of an isolated noise source (Schippkus et al., 2022) that repeatedly excites a wavelet to illustrate the fundamental principle of how repeated direct waves emerge in correlation functions (Figs. 3, 5). To better reproduce the measurements on field data correlations, we model an isolated secondary microseism source, starting with one source (Fig. 7), which shows a distinct main arrival of that source (the "spurious arrival") that is not always observed clearly on field data correlations. With a cluster of isolated noise sources, mimicking an extended source region, this main arrival disappears due to interference between the sources (Fig. 8). Finally, we model two clusters to show that either may be detected at a given lapse time (Fig. 9), reliably reproducing the observations on our field data correlation wavefields (Figs. 1, 2). Throughout our modelling, we keep the numerical setup as simple as possible to emphasise the impact of only the isolated noise sources, i.e., we exclude any influence due to heterogeneous Earth structure, any elastic wave propagation effects such as multiple wave types or conversion between them, and importantly do not include any scattering.

Our results suggest that the coda of correlation wavefields should not be assumed to be mainly comprised of scattered waves, which originated from the master station. Instead, repeating direct waves from isolated noise sources may dominate. There is likely a transition in dominating regime from scattered waves (in the early coda) to repeating direct waves (in the late coda). This occurs, because amplitudes of scattered waves decay due to attenuation, whereas repeating direct waves decay slower only due to the auto-correlation of the source term throughout time. This has implications for ambient noise correlation based monitoring applications, commonly assuming multiply scattered waves, and raises questions about the validity of such measurements, in particular about the spatial sensitivity.

This study also opens up new opportunities for future research. In the presence of a continuously acting isolated noise source, the very late coda of correlation wavefields retains the source signature and is not dominated by instrument noise. This in principle allows to extract seismic waves repeatedly propagating along the same path, undisturbed by other contributions, which may be an attractive target for monitoring applications. The spatial distribution of isolated noise sources, however, severely limits the spatial sensitivity of the very late correlation wavefield coda.

Data Availability and Resources

This manuscript is fully reproducible. All computed correlation functions and code necessary to produce all figures are hosted on Github and Zenodo (Schippkus, 2023). Seismograms used in this study to compute correlation functions are provided by the network operators of the German Regional Seismic Network (GR, Federal Institute for Geosciences and Natural Resources, 1976), Polish Seismological Network (PL, Polish Academy of Sciences (PAN) Polskiej Akademii Nauk, 1990), and Italian National Seismic Network (IV, Istituto Nazionale di Geofisica e Vulcanologia (INGV), 2005). We rely on open-source software for our computations and visualisations (Hunter, 2007; Met Office, 2010; Krischer et al., 2015; Harris et al., 2020; Virtanen et al., 2020). Color sequences are designed to be accessible (Petroff, 2021).

Acknowledgements

The authors thank Joshua Russel and one anonymous reviewer for their insightful comments that helped improve the manuscript, as well as the handling editor Lise Retailleau. The authors acknowledge funding provided by the Emmy Noether program (HA7019/1-1) of the German Research Foundation (DFG). The authors acknowledge funding provided by the European Union's Horizon 2020 research and innovation programme under the Marie Skłodowska-Curie grant agreement No. 955515 (SPIN ITN).

References

G. D. Bensen, M. H. Ritzwoller, M. P. Barmin, A. L. Levshin, F. Lin, M. P. Moschetti, N. M. Shapiro, and Y. Yang. Processing seismic ambient noise data to obtain reliable broad-band surface wave dispersion measurements. *Geophysical Journal International*, 169(3):1239–1260, June 2007. ISSN 0956-540X. doi: 10.1111/j.1365-246X.2007.03374.x.

C. Bruland and C. Hadziioannou. Gliding tremors associated with the 26 second microseism in the Gulf of Guinea. *Communications Earth & Environment*, 4(1):1–9, May 2023. ISSN 2662-4435. doi: 10.1038/s43247-023-00837-y.

S. Chevrot, M. Sylvander, S. Benahmed, C. Ponsolles, J. M. Lefèvre, and D. Paradis. Source locations of secondary microseisms in western Europe: Evidence for both coastal and pelagic sources. *Journal of Geophysical Research: Solid Earth*, 112(B11), Nov. 2007. ISSN 2156-2202. doi: 10.1029/2007JB005059.

Federal Institute for Geosciences and Natural Resources. German Regional Seismic Network (GRSN), 1976.

A. Friedrich, F. Krüger, K. Klinge, and 1998. Ocean-generated microseismic noise located with the Gräfenberg array. *Journal of Seismology*, 2:47–64, 1998. doi: 10.1023/A:1009788904007.

T. Friedrich, T. Zieger, T. Forbriger, and J. R. R. Ritter. Locating wind farms by seismic interferometry and migration. *Journal of Seismology*, 22(6):1469–1483, Nov. 2018. ISSN 1573-157X. doi: 10.1007/s10950-018-9779-0.

P. Gouédard, L. Stehly, F. Brenguier, M. Campillo, Y. Colin de Verdière, E. Larose, L. Margerin, P. Roux, F. J. Sánchez-Sesma, N. M. Shapiro, and R. L. Weaver. Cross-correlation of random fields: Mathematical approach and applications. *Geophysical Prospecting*, 56(3):375–393, 2008. ISSN 1365-2478. doi: 10.1111/j.1365-2478.2007.00684.x.

L. Gualtieri, E. Bachmann, F. J. Simons, and J. Tromp. The origin of secondary microseism Love waves. *Proceedings of the National Academy of Sciences of the United States of America*, 117(47):29504–29511, Nov. 2020. doi: 10.1073/pnas.2013806117.

C. Hadziioannou, E. Larose, O. Coutant, P. Roux, and M. Campillo. Stability of monitoring weak changes in multiply scattering media with ambient noise correlation: Laboratory experiments. *The Journal of the Acoustical Society of America*, 125(6):3688–3695, June 2009. ISSN 0001-4966. doi: 10.1121/1.3125345.

C. R. Harris, K. J. Millman, S. J. van der Walt, R. Gommers, P. Virtanen, D. Cournapeau, E. Wieser, J. Taylor, S. Berg, N. J. Smith, R. Kern, M. Picus, S. Hoyer, M. H. van Kerkwijk, M. Brett, A. Haldane, J. F. del Río, M. Wiebe, P. Peterson, P. Gérard-Marchant, K. Sheppard, T. Reddy, W. Weckesser, H. Abbasi, C. Gohlke, and T. E. Oliphant. Array programming with NumPy. *Nature*, 585(7825):357–362, Sept. 2020. doi: 10.1038/s41586-020-2649-2.

J. D. Hunter. Matplotlib: A 2D graphics environment. *Computing in Science & Engineering*, 9(3):90–95, 2007. doi: 10.1109/MCSE.2007.55.

Istituto Nazionale di Geofisica e Vulcanologia (INGV). Rete Sismica Nazionale (RSN), 2005.

C. Juretzek and C. Hadziioannou. Where do ocean microseisms come from? A study of Love-to-Rayleigh wave ratios. *Journal of Geophysical Research: Solid Earth*, 121(9):6741–6756, Sept. 2016. doi: 10.1002/2016JB013017.

L. Krischer, T. Megies, R. Barsch, M. Beyreuther, T. Lecocq, C. Caudron, and J. Wassermann. ObsPy: A bridge for seismology into the scientific Python ecosystem. *Computational Science & Discovery*, 8(014003), Jan. 2015. doi: 10.1088/1749-4699/8/1/014003.

O. I. Lobkis and R. L. Weaver. Coda-Wave Interferometry in Finite Solids: Recovery of P -to- S Conversion Rates in an Elastodynamic Billiard. *Physical Review Letters*, 90(25):254302, June 2003. ISSN 0031-9007, 1079-7114. doi: 10.1103/PhysRevLett.90.254302.

Y. Lu, L. Stehly, A. Paul, and the AlpArray Working Group. High-resolution surface wave tomography of the European crust and uppermost mantle from ambient seismic noise. *Geophysical Journal International*, 214(2):1136–1150, May 2018. doi: 10.1093/gji/ggy188.

S. Mao, A. Lecointre, R. D. van der Hilst, and M. Campillo. Space-time monitoring of groundwater fluctuations with passive seismic interferometry. *Nature Communications*, 13(1):4643, Aug. 2022. ISSN 2041-1723. doi: 10.1038/s41467-022-32194-3.

L. Margerin, T. Planès, J. Mayor, and M. Calvet. Sensitivity kernels for coda-wave interferometry and scattering tomography: Theory and numerical evaluation in two-dimensional anisotropically scattering media. *Geophysical Journal International*, 204(1):650–666, Jan. 2016. ISSN 0956-540X. doi: 10.1093/gji/ggv470.

Met Office. *Cartopy: A Cartographic Python Library with a Matplotlib Interface*. Exeter, Devon, 2010.

S. Nagel, T. Zieger, B. Luhmann, P. Knödel, J. Ritter, and T. Ummenhofer. Ground motions induced by wind turbines. *Civil Engineering Design*, 3(3):73–86, 2021. ISSN 2625-073X. doi: 10.1002/cend.202100015.

A. Obermann, B. Froment, M. Campillo, E. Larose, T. Planès, B. Valette, J. H. Chen, and Q. Y. Liu. Seismic noise correlations to image structural and mechanical changes associated with the Mw 7.9 2008 Wenchuan earthquake. *Journal of Geophysical Research: Solid Earth*, 119(4): 3155–3168, Apr. 2014. ISSN 2169-9356. doi: 10.1002/2013JB010932.

M. A. Petroff. Accessible Color Sequences for Data Visualization. July 2021. doi: 10.48550/arXiv.2107.02270.

T. Planès, E. Larose, L. Margerin, V. Rossetto, and C. Sens-Schönfelder. Decorrelation and phase-shift of coda waves induced by local changes: Multiple scattering approach and numerical validation. *Waves in Random and Complex Media*, 24(2):99–125, Apr. 2014. ISSN 1745-5030. doi: 10.1080/17455030.2014.880821.

Polish Academy of Sciences (PAN) Polskiej Akademii Nauk. Polish Seismological Network, 1990.

L. Retailleau, P. Boué, L. Stehly, and M. Campillo. Locating Microseism Sources Using Spurious Arrivals in Intercontinental Noise Correlations. *Journal of Geophysical Research: Solid Earth*, 122(10):8107–8120, 2017. ISSN 2169-9356. doi: 10.1002/2017JB014593.

S. Rost and C. Thomas. Array Seismology: Methods and Applications. *Reviews of Geophysics*, 40(3):2–1–2–27, 2002. ISSN 1944-9208. doi: 10.1029/2000RG000100.

S. Schippkus. Schipp/repeating_direct_waves: V0.1 - pre-print prep. Feb. 2023. doi: 10.5281/zenodo.7643286.

S. Schippkus, D. Zigone, G. H. R. Bokelmann, and the AlpArray Working Group. Ambient-noise tomography of the wider Vienna Basin region. *Geophysical Journal International*, 215(1):102–117, June 2018. doi: 10.1093/gji/ggy259.

S. Schippkus, M. Garden, and G. Bokelmann. Characteristics of the Ambient Seismic Field on a Large-N Seismic Array in the Vienna Basin. *Seismological Research Letters*, 91(5):2803–2816, July 2020. ISSN 0895-0695. doi: 10.1785/0220200153.

S. Schippkus, R. Snieder, and C. Hadziioannou. Seismic interferometry in the presence of an isolated noise source. *Seismica*, 1(1), Dec. 2022. ISSN 2816-9387. doi: 10.26443/seismica.v1i1.195.

C. Sens-Schönfelder and E. Larose. Lunar noise correlation, imaging and monitoring. *Earthquake Science*, 23(5):519–530, Oct. 2010. doi: 10.1007/s11589-010-0750-6.

Y. Sheng, A. Mordret, F. Brenguier, P. Boué, F. Vernon, T. Takeda, Y. Aoki, T. Taira, and Y. Ben-Zion. Seeking Repeating Anthropogenic Seismic Sources: Implications for Seismic Velocity Monitoring at Fault Zones. *Journal of Geophysical Research: Solid Earth*, 128(1), Jan. 2023. ISSN 2169-9313, 2169-9356. doi: 10.1029/2022JB024725.

R. Snieder, K. Wapenaar, and K. Larner. Spurious multiples in seismic interferometry of primaries. *GEOPHYSICS*, 71(4):SI111–SI124, July 2006. ISSN 0016-8033. doi: 10.1190/1.2211507.

D. Soergel, H. A. Pedersen, T. Bodin, A. Paul, L. Stehly, AlpArray Working Group, G. Hetényi, R. Abreu, I. Allegretti, M.-T. Apoloner, C. Aubert, M. Bes De Berc, G. Bokelmann, D. Brunel, M. Capello, M. Cărman, A. Cavaliere, J. Chèze, C. Chiarabba, J. Clinton, G. Cougoulat, W. Crawford, L. Cristiano, T. Czifra, E. D'Alema, S. Danesi, R. Daniel, I. Dasović, A. Deschamps, J.-X. Dessa, C. Doubre, and S. Egdorf. Bayesian analysis of azimuthal anisotropy in the Alpine lithosphere from beamforming of ambient noise cross-correlations. *Geophysical Journal International*, 232(1):429–450, Sept. 2022. ISSN 0956-540X, 1365-246X. doi: 10.1093/gji/ggac349.

D. Sollberger, N. Bradley, P. Edme, and J. O. A. Robertsson. Efficient wave type fingerprinting and filtering by six-component polarization analysis. *Geophysical Journal International*, 234(1):25–39, Feb. 2023. ISSN 0956-540X. doi: 10.1093/gji/ggad071.

C. van Dinther, L. Margerin, and M. Campillo. Implications of Laterally Varying Scattering Properties for Subsurface Monitoring With Coda Wave Sensitivity Kernels: Application to Volcanic and Fault Zone Setting. *Journal of Geophysical Research: Solid Earth*, 126(12), Dec. 2021. ISSN 2169-9313, 2169-9356. doi: 10.1029/2021JB022554.

P. Virtanen, R. Gommers, T. E. Oliphant, M. Haberland, T. Reddy, D. Cournapeau, E. Burovski, P. Peterson, W. Weckesser, J. Bright, S. J. van der Walt, M. Brett, J. Wilson, K. J. Millman, N. Mayorov, A. R. J. Nelson, E. Jones, R. Kern, E. Larson, C. J. Carey, İ. Polat, Y. Feng, E. W. Moore, J. VanderPlas, D. Laxalde, J. Perktold, R. Cimrman, I. Henriksen, E. A. Quintero, C. R. Harris, A. M. Archibald, A. H. Ribeiro, F. Pedregosa, P. van Mulbregt, and SciPy 1.0 Contributors. SciPy 1.0: Fundamental algorithms for scientific computing in python. *Nature Methods*, 17: 261–272, 2020. doi: 10.1038/s41592-019-0686-2.

K. Wapenaar, J. Fokkema, and R. Snieder. Retrieving the Green's function in an open system by cross correlation: A comparison of approaches (L). *The Journal of the Acoustical Society of America*, 118(5):2783–2786, Nov. 2005. ISSN 0001-4966. doi: 10.1121/1.2046847.

U. Wegler and C. Sens-Schönfelder. Fault zone monitoring with passive image interferometry. *Geophysical Journal International*, 168(3): 1029–1033, Mar. 2007. ISSN 0956-540X. doi: 10.1111/j.1365-246X.2006.03284.x.

A. Yates, C. Caudron, P. Lesage, A. Mordret, T. Lecocq, and J. Soubestre. Assessing similarity in continuous seismic cross-correlation functions using hierarchical clustering: Application to Ruapehu and Piton de la Fournaise volcanoes. *Geophysical Journal International*, 233 (1):472–489, Nov. 2022. ISSN 0956-540X, 1365-246X. doi: 10.1093/gji/ggac469.

X. Zeng and S. Ni. A persistent localized microseismic source near the Kyushu Island, Japan. *Geophysical Research Letters*, 37(24), 2010. ISSN 1944-8007. doi: 10.1029/2010GL045774.